CW-115380-CONF-016 Rev D1 / UNRESTRICTED

Benchmarking MAAP-CANDU v4.0.7B with GOTHIC 7.2b: Response of Containment Models to Flashing and Condensation

M.J. Brown[1], Y-S. Chin[1], S. Gyepi-Garbrah[2]
[1] Canadian Nuclear Laboratories Limited (CNL), Chalk River, Ontario, Canada
[2] Canadian Nuclear Safety Commission, Ottawa, Ontario, Canada
morgan.brown@cnl.ca

Abstract

Containment is the last line of defence in a reactor accident, preventing radioactive releases to the public, so well-modelled containment behaviour is important. MAAP-CANDU is an integrated severe accident simulation code of the CANDU Owners Group Industry Standard Toolset; it has model simplifications, limited nodalization and lumped-parameter containment models. GOTHIC is a generalized thermalhydraulic code, also part of the IST, used for more sophisticated containment modelling.

Water + steam injections to a single containment node are modelled, with and without a heat sink, comparing MAAP-CANDU to GOTHIC (lumped containment models). For LOCA break conditions, both codes predict similar heat and mass transfer rates, with minor differences, when the GOTHIC flashing model is configured similar to that of MAAP-CANDU. However, when the recommended flashing model is used in GOTHIC, larger differences are observed, including lower pressures and vapour temperatures and higher steam concentrations in GOTHIC.

Keywords: MAAP-CANDU, GOTHIC, containment modeling

1. Introduction

Severe accidents in nuclear reactors have lower probabilities but higher consequences than design-basis accidents, and could cause fission products (FP) to be released to the environment, posing risks to health, the environment, and the economy. Three Mile Island-2 (1979, USA), Chernobyl-4 (1986, Ukraine) and Fukushima Daiichi (2011, Japan) showed that severe accidents can have significant consequences. Understanding severe accident phenomena, as well as simulating accidents and interpreting results, is necessary for Probabilistic Safety Assessment and for determining Severe Accident Management (SAM) strategies.

MAAP-CANDU is an integrated severe accident code, developed by Fauske and Associates Inc (FAI) and the Canadian nuclear industry, to simulate postulated severe accidents in CANDU plants [1]. It is part of the MAAP suite of severe accident codes, owned by the Electric Power Research Institute (EPRI), and shares many models with MAAP-LWR codes. MAAP-CANDU development, licensing, documentation and quality assurance (QA) is managed by the CANDU Owners Group (COG), and the code is part of the COG Industry Standard Toolset (IST). This paper focuses on the containment models common to all MAAP codes.

Canadian Nuclear Laboratories (CNL, formerly Atomic Energy of Canada Limited) has two decades of MAAP-CANDU experience, performing analytical and experimental work to support model/code development, code QA, and documentation. CNL provides code assistance to the

Canadian Nuclear Safety Commission (CNSC), which uses MAAP-CANDU to assess licensing applications and evaluate SAM strategies. A joint CNL/CNSC program led to the development (by FAI) of an interactive animation package for MAAP-CANDU [2].

GOTHIC is a thermalhydraulics computer program for the design, licensing, and safety analysis of nuclear reactor containments [3], and is also a COG IST code. GOTHIC is also owned by EPRI, and is developed by NAI (Numerical Applications, Inc.).

This paper describes six containment benchmarks performed by CNL and the CNSC, comparing MAAP-CANDU v4.0.7B with GOTHIC v7.2b and also an analytical solution. Details of some MAAP-CANDU models are presented to help understand containment behaviour.

2. Background

MAAP-CANDU predicts severe accident progression starting with a set of nuclear plant system faults and initiating events that could lead to severe core damage. The code calculates the overall plant response, including the heat-up and damage progression in the core and surrounding structures, plus FP release, transport, and deposition in the plant and environment. MAAP-CANDU simulates the fuel channels, primary heat transport system (PHTS), calandria vessel, safety systems and containment. It is fast-running, modelling many processes and phenomena with simplified assumptions, and with mechanistic and parametric models. Code experience and validation shows input can be adjusted so MAAP-CANDU better emulates more mechanistic codes and analytical models, such as during the PHTS blowdown phase [4].

MAAP-CANDU v4.0.7 containment simulation results were previously compared with those of GOTHIC v7.2b, using the GOTHIC lumped-parameter model rather than its 3-D model. A CANDU 6 station blackout accident was simulated with containment dousing either credited [5] or not [6]. Mass and energy inputs to GOTHIC (lumped parameter model) were generated with MAAP-CANDU, and both containment nodalizations were identical. The code comparison showed reasonable agreement for parameters like containment pressure and temperatures, particularly for parameter trends. However, it was difficult to ensure all appropriate system boundary conditions and inputs were transferred from MAAP-CANDU to GOTHIC, and the complexity of containment and the accident sequence made it difficult to compare code models.

Thus more basic comparisons of the two codes were performed, using the MAAP-CANDU containment benchmarking capability and injecting steam / water into a single large volume. This study uses containment pressure as a figure-of-merit - either peak pressure after the flashing jet ceases, or final pressure after a period of condensation or superheated steam injection.

3. Containment Compartment (Node 8)

The containment compartment, common to the MAAP-CANDU and GOTHIC simulations, is Node 8 from the generic CANDU 6 parameter file (station description) used in references [5] and [6]. Node 8 is a rectangular volume of 19,809 m^3 and 15.55 m high. It is isolated by closing all junctions and removing all heat sinks (walls, ceiling, floor and internal structures) except Heat Sink 65. By being isolated, the code models for flashing jet, pool evaporation, convection and condensation can be evaluated separately. Heat Sink 65 (vertical, single-sided, 1,000 m^2, 0.2 m thick, 10 m high) is active only in Benchmarks 4 to 6 to test convection and condensation heat transfer models. Heat Sink 65 is ordinary concrete (c_p = 840 J/(kg-K), k = 1.38 W/(m-K), ρ = 2,300 kg/m^3), and heat transfer occurs only on the one side exposed to Node 8.

4. Containment Benchmark Simulations

Six benchmarks were performed with MAAP-CANDU and GOTHIC modelling steam/water injection into a large, empty (no initial water), isolated and adiabatic volume. Some benchmarks use multiple GOTHIC runs for different flashing jet model assumptions. Light water properties are used (MAAP-CANDU only has light water properties).

Table 1: Benchmark conditions

Benchmark	Injection	Heat sink	Node initial conditions
1 Superheated steam jet	10,000 s of 28 kg/s steam (superheated 2.793 MJ/kg)	None	101 kPa, 32°C Dry (RH=0%)
2 Flashing jet (1800 s)	1800 s of 70 kg/s water (saturated 1.407 MJ/kg)	None	101 kPa, 32°C Dry (RH=0%)
3 Flashing jet (RIH break)	Simulated CANDU 6 35% RIH break (107 s discharge)	None	101 kPa, 32°C Dry (RH=0%)
4 Quiescent volume with heat sink	None. Condensation and cooling of Node 8 by heat sink	Vertical concrete wall, 10 m tall, 0.2 m thick, 1000 m^2	300 kPa, 133.5°C Humid (RH=60%) Heat sink 65=25°C
5 Flashing jet (1800 s) with heat sink	1800 s discharge of 70 kg/s water at 1.407 MJ/kg	Vertical concrete wall, 10 m tall, 0.2 m thick, 1000 m^2	101 kPa, 32°C Dry (RH=0%) Heat sink 65=25°C
6 Flashing jet (RIH break) with heat sink	Simulated CANDU 6 35% RIH break (107 s discharge)	Vertical concrete wall, 10 m tall, 0.2 m thick, 1000 m^2	101 kPa, 32°C Dry (RH=0%) Heat sink 65=25°C

4.1 Benchmark 1: Steam Injection

Benchmark 1 is a continuous injection of 28 kg/s of superheated steam (h_{stm} = 2.793 MJ/kg) for 10,000 s, emulating high-pressure steam discharged from a CANDU PHTS liquid relief valve; the exact conditions are not important, provided it is well-superheated steam (ideal gas).

An analytical solution was also run for a period of 500 s. Assuming uniform properties at the inlet and outlets (i.e., uniform-state uniform-flow process), the generalized first law of thermodynamics for a control volume is:

$$\dot{Q}_{CV} + \sum \dot{m}_i \left(h_i + \frac{V_i^2}{2} + gZ_i \right) = \frac{dE_{CV}}{dt} + \sum \dot{m}_e \left(h_e + \frac{V_e^2}{2} + gZ_e \right) + \dot{W}_{CV} \tag{1}$$

The control volume is adiabatic ($\dot{Q}_{CV} = 0$) with no exit flow ($\dot{m}_e = 0$) and no work is performed ($\dot{W}_{CV} = 0$). The inlet kinetic energy $\frac{V_i^2}{2}$ and potential energy gZ_i were assumed insignificant so

$$\dot{m}_i h_i = \frac{dE_{CV}}{dt} = \frac{d\left(m\left(u_{CV} + \frac{V_{CV}^2}{2} + gZ_{CV}\right)\right)}{dt} \tag{2}$$

By integrating and assuming the kinetic and potential energy within the control volume are negligible, the energy balance over a discrete time step ($\Delta t = t_2 - t_1$) is:

$$m_i h_i = m_2 u_2 - m_1 u_1 \tag{3}$$

The control volume is a mixture of air and steam. Assuming the air energy is proportional to the temperature ($u_{air} = c_{vair} T$), and the specific heat c_{vair} and mass of air in the control volume are constant ($m_{air2} = m_{air1} = m_{air}$), the first law becomes:

$$m_i h_i + m_{stm1} u_{stm1} + m_{air} c_{vair} T_1 = m_{stm2} u_{stm2} + m_{air} c_{vair} T_2 \tag{4}$$

The left side of Equation 4 is known from node and flow conditions at the start of the time step. With the updated total steam mass m_{stm2}, and assuming temperature T_2, steam partial pressure P_{stm2} is solved. The specific internal energy u_{stm2} is determined from steam tables at T_2 and P_{stm2}. Gas temperature T_2 is iterated until Equation 4 balances, and the solution is advanced by 1 s. The solution is limited to 500 s since the results are virtually identical to those from MAAP-CANDU and GOTHIC (Figure 1). The peak in relative humidity (54% at 42 s) is due to the steam partial pressure, because at low temperatures dP_{sat}/dT is low. Increasing the initial node temperature or relative humidity would decrease or eliminate the peak in the relative humidity.

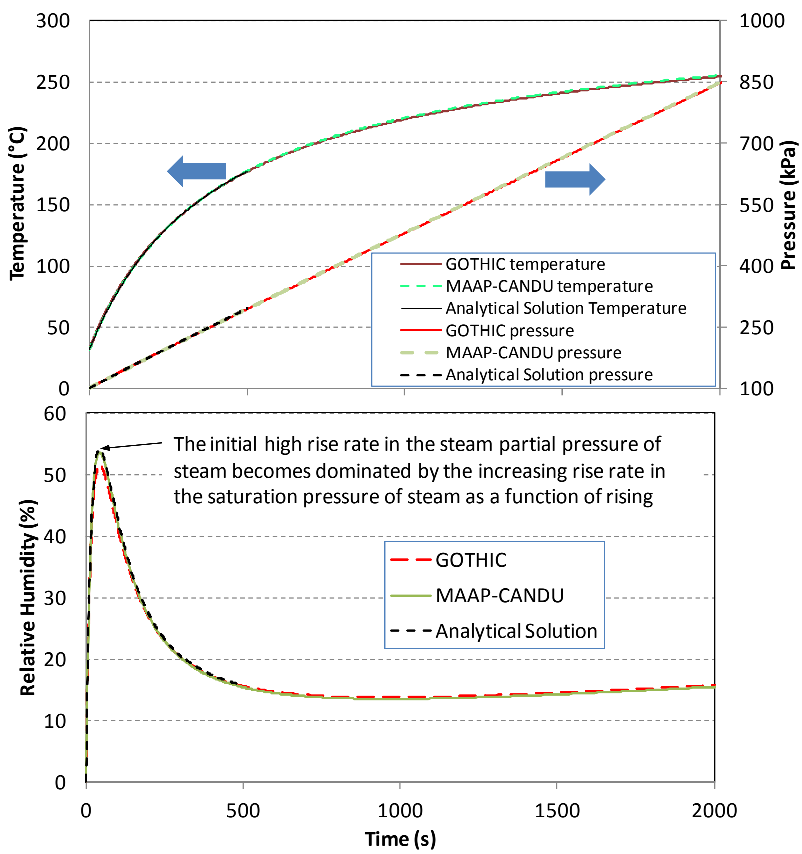

Figure 1 Benchmark 1: Node 8 pressure, temperature, relative humidity - 28 kg/s steam injection

4.2 Benchmarks 2 and 3: Flashing Jet Injection

Benchmarks 2 and 3 model a saturated water injection into Node 8, where some water flashes to steam. These benchmarks are complex so only MAAP-CANDU and GOTHIC are compared.

4.2.1 Benchmark 2: Steady-State Flashing Jet

In Benchmark 2 a jet of 70 kg/s ($\dot{m}_i$) of 1,407,000 J/kg (h_i) water is injected into Node 8 for 1,800 s. The enthalpy corresponds to saturation at CANDU reactor outlet conditions (10.0 MPa). In Node 8 (101.0 kPa) the saturated liquid enthalpy is 419,000 J/kg and the saturated vapour enthalpy is 2,676,000 J/kg. MAAP-CANDU assumes the injected flow remains at a constant total enthalpy, dividing into:

a) water mass flow $\dot{m}_f$ at saturation at the downstream pressure (enthalpy h_f), and
b) steam mass flow (flashing rate) $\dot{m}_g$ at saturation at downstream pressure (enthalpy h_g).

From the conservation of mass and energy, and rearranging for the flashing rate $\dot{m}_g$:

$$\dot{m}_g = \dot{m}_i \left(\frac{h_i - h_f}{h_g - h_f} \right) \tag{5}$$

Initially the jet flashes to 31 kg/s of saturated steam and 39 kg/s of saturated water. The steam partial pressure increases from 0 kPa and the atmosphere heats up, increasing the partial air pressure. The water does not cool by contact with the floor because the node is modelled as adiabatic. As Node 8 heats up and pressurizes, the saturation conditions change so the flashing rate decreases. The pool is hot, and Node 8 is initially dry and cool, so pool water evaporates.

The Schmidt number ($\mathrm{Sc} = \mu/(\rho D)$) for mass transfer is analogous to the Prandtl number ($\mathrm{Pr} = c_p \mu / k$) for convective heat transfer: D is the mass diffusion coefficient, μ the dynamic viscosity, ρ the fluid density, c_p the fluid specific heat, and k the fluid thermal conductivity. The Lewis number Le (=Sc/Pr) is equal to the ratio of the thermal and mass diffusivities. For Le~1, the effects due to temperature and steam concentration differences are additive.

For turbulent convective heat transfer above a horizontal surface (no mass transfer), MAAP-CANDU uses the following Nusselt number correlation derived from experimental results [7]:

$$\mathrm{Nu_h} = \frac{L\, \ddot{q}_{conv}}{k(T_w - T_\infty)} = 0.156\, (\mathrm{Gr_h\, Pr})^{1/3} \tag{6}$$

where $\ddot{q}_{conv}$ is the heat flux and L is a characteristic length. Subscripts $_w$ and $_\infty$ indicate gas at pool surface and ambient conditions. The heat transfer Grashof number is:

$$\mathrm{Gr_h} = \frac{g\, \beta_h\, L^3\, (T_w - T_\infty)}{\nu^2} \tag{7}$$

where β_h is the volume coefficient of thermal expansion ($=1/T_\infty$), g is gravitational acceleration and ν is the kinematic viscosity ($= \mu/\rho$). The mass transfer Nusselt number (Sherwood number) is similar to Equation 6, where $\ddot{m}_{evap}$ is the evaporation mass flux from the pool surface and D is the diffusion coefficient of steam in air.

CW-115380-CONF-016 Rev D1 / UNRESTRICTED

$$\mathrm{Nu_m} = \frac{L\,\ddot{m}_{evap}}{D\rho\,(Y_w - Y_\infty)} = 0.156\,(\mathrm{Gr_m\,Sc})^{1/3} \tag{8}$$

The difference in steam mass fraction $(Y_w - Y_\infty)$, between pool surface and ambient conditions, drives the mass transfer,. The mass transfer Grashof number is:

$$\mathrm{Gr_m} = \frac{g\,\beta_m\,L^3\,(Y_w - Y_\infty)}{\nu^2} \tag{9}$$

β_m is the concentration coefficient of thermal expansion, and M is the molecular weight:

$$\beta_\mathrm{m} = \frac{M_\infty - M_{stm}}{M_{stm}} \tag{10}$$

Since Le~1, the heat transfer Grashof number in Equation 6 can be replaced by the combined Grashof number for heat transfer and mass transfer, $\mathrm{Gr_h} + \mathrm{Gr_m}$:

$$\begin{aligned}\mathrm{Nu_h} &= 0.156\,(\mathrm{Gr_h\,Pr} + \mathrm{Gr_m\,Sc})^{1/3}, \text{ and}\\ \mathrm{Nu_m} &= 0.156\,(\mathrm{Gr_h\,Pr} + \mathrm{Gr_m\,Sc})^{1/3}\end{aligned} \tag{11}$$

Substituting for the Grashof, Prandtl and Schmidt numbers, and rearranging the Nusselt numbers to solve for the convective heat and evaporative mass fluxes:

$$\begin{aligned}\ddot{q}_{conv} &= 0.156\,\frac{k(T_w - T_\infty)}{\left[{}^{\alpha\,\nu}/_{g}\right]^{\frac{1}{3}}}\left[\frac{T_w - T_\infty}{T_\infty} + (Y_w - Y_\infty)\,\frac{M_\infty - M_{stm}}{M_{stm}}\right]^{\frac{1}{3}}\\ \ddot{m}_{evap} &= 0.156\,\frac{D\rho\,(Y_w - Y_\infty)}{\left[{}^{\alpha\,\nu}/_{g}\right]^{\frac{1}{3}}}\left[\frac{T_w - T_\infty}{T_\infty} + (Y_w - Y_\infty)\,\frac{M_\infty - M_{stm}}{M_{stm}}\right]^{\frac{1}{3}}\end{aligned} \tag{12}$$

Initially the water pool increases at 39 kg/s, the water temperature T_W is 100°C, the steam mass fraction above the pool Y_W = 1.0, the ambient steam mass fraction Y_∞=0.0, and the ambient gas temperature T_∞ = 32°C. The heat flux from the pool $\ddot{q}_{conv}$ = 755 W/m^2 and the evaporation flux $\ddot{m}_{evap}$= 0.0143 kg/(m^2 s). For a surface area of 1,274 m^2, the convective heat transfer rate $\dot{q}_{conv}$ = 96.6 kW and the evaporation rate $\dot{m}_{evap}$ = 18.2 kg/s. The convection is from water to air, ignoring mass transfer; the evaporating water transfers additional heat to the air:

$$\dot{q}_{evap} = \dot{m}_{evap} h_g \tag{13}$$

Thus initially $\dot{q}_{conv}$ = 48.7 MW. The pool cools by evaporation, but at $\dot{m}_{evap}$=18.2 kg/s it would freeze. Within MAAP-CANDU, error checking limits the mass transfer, typically only during the first few time steps (a fraction of a second). As the pool mass increases, the evaporation rate can increase to the value calculated by Equation 12.

The flashing jet increases the steam and water in Node 8, while the pool cools by evaporation. If the pool cooled to T_W=99°C, the steam just above the pool would have a partial pressure of 97.5 kPa at T_W, and a density of 0.58 kg/m^3. The air density at T_W and 3.5 kPa is 0.0330 kg/m^3. Therefore the steam mass fraction Y_W drops to 0.946 while Y_∞ remains at ~0.0. From Equation 12, the decreases in $(Y_w - Y_\infty)$ and $(T_w - T_\infty)$ cause a 3% drop in convective heat transfer and a

7% drop in evaporation rate, due to a 1°C drop in the pool temperature; if the increases in ambient conditions are taken into account, the heat transfer and evaporation decrease further.

The Node 8 masses of steam and water are shown for MAAP-CANDU and two of the GOTHIC simulations (Figure 2). The steam-to-water mass ratio drops from ~0.87 to ~0.70 by 700 s and stays virtually constant for the rest of the simulation, because: a) flashing decreases as the node pressure increases, and b) the evaporation rate decreases as the pool cools and the ambient steam mass fraction increases. After the injection ceases (1,800 s) a small amount of pool water evaporates to try to attain equilibrium within the node.

Five cases compare different GOTHIC flashing models to the single MAAP-CANDU model:

- Case 1a: The entire jet enters Node 8 as 100 micron droplets at 10 MPa. Droplets flash upon entering Node 8. A "near-equilibrium" model.
- Case1b: The jet flashes at the Node 8 pressure. The resulting flows enter Node 8 as saturated steam, plus saturated liquid as 100 micron droplets. This "near-equilibrium" model is recommended by the GOTHIC developer NAI.
- Case 1c: The entire jet enters the Node 8 water pool as 10 MPa water (no droplets); the pool water then flashes. A "non-equilibrium" model.
- Case 1c-Forced Equilibrium: The same as Case 1c except the "Forced Equilibrium" setting is selected. GOTHIC attempts to ensure thermal equilibrium between the phases.
- Case 1d: Like Case 1b, the jet flashes at the Node 8 pressure. The resulting flows enter Node 8 as saturated steam, plus saturated liquid, all of which enters the water pool (i.e., no droplets). A "non-equilibrium" model that closely resembles the MAAP-CANDU model.

GOTHIC Case 1c generates more water and less steam than Case 1d, and results are similar to MAAP-CANDU (Figure 2). In the GOTHIC cases, the conditions in brackets represent the fluid, Case number, flashing pressure, and droplet diameter.

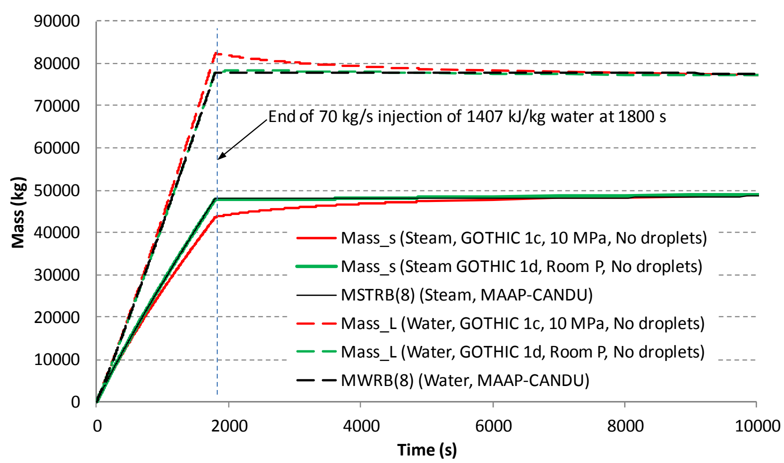

Figure 2 Benchmark 2: Node 8 steam and water masses - 70 kg/s flashing jet.

The MAAP-CANDU and GOTHIC Case 1d temperatures (Figure 3) show the initial 100°C water pool rapidly cools to ~70°C by evaporation and convection. The rising ambient gas temperature decreases convective losses, while the rising steam partial pressure decreases evaporation. The water pool temperature increases again, reaching 144.2°C (MAAP-CANDU) or 145.8°C (GOTHIC) by the end of the injection period. The water temperatures continue to rise slowly because convection from the hot ambient gas exceeds the decreasing evaporation.

The saturation temperature (Figure 3), based on the steam partial pressure, is the dew point, below which steam condenses. The gas exceeds the dew point for the entire simulation, so no condensation occurs. Temperature and concentration gradients can be in opposite directions in Equation 12; e.g., water will evaporate if $T_\infty > T_w$ and $Y_w - Y_\infty > 0$, and the following is true:

$$(Y_w - Y_\infty)\frac{M_\infty - M_{stm}}{M_{stm}} \geq -\left(\frac{T_w - T_\infty}{T_\infty}\right) \tag{14}$$

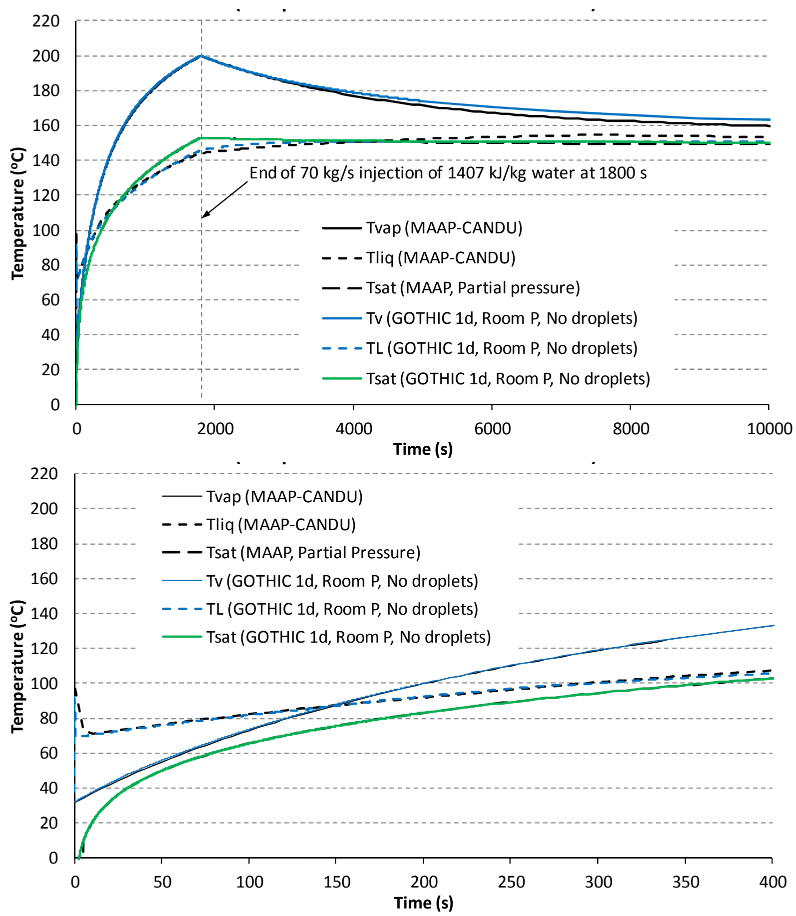

Figure 3 Benchmark 2: Node 8 gas (steam + air) and water temperatures - 70 kg/s flashing jet.

The relative humidities in the MAAP-CANDU and GOTHIC Case 1d simulations (Figure 4) are close, similar to Benchmark 1 (Figure 1). GOTHIC Cases 1a, 1b and 1c-Forced Equilibrium show a rapid increase in relative humidity to 100%. This is expected, since Cases 1a and 1b model the jet as flashing steam plus 100 micron droplets; the very large surface area means the liquid rapidly evaporates to saturate the air. Case 1c-Forced Equilibrium attempts to equilibrate between the phases, so it also rapidly reaches saturation. Case 1c (i.e., not Forced Equilibrium) assumes the entire jet is added to the water pool at 10 MPa, which then flashes to steam; this initially saturates the air, but also forces the ambient air to heat up faster, so the relative humidity drops. Given that Node 8 is very large (19,809 m^3), it is unlikely that the node average relative humidity would so rapidly increase to 100%. When using lumped parameter models for a large node, GOTHIC Cases 1a, 1b, 1c and 1c-Forced Equilibrium seem improbable.

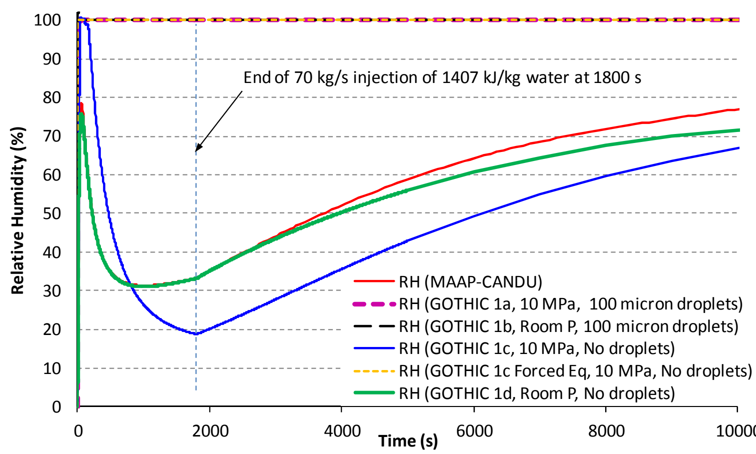

Figure 4 Benchmark 2: Node 8 relative humidity - 70 kg/s flashing jet.

The containment peak pressures (Figure 5) all occur at the end of the injection (1,800 s), and then gradually decline. The "non-equilibrium" MAAP-CANDU and GOTHIC 1c and 1d simulations generate the highest peak pressures of 0.674 MPa, 0.668 MPa and 673 MPa, respectively. The lowest peak pressure (0.610 MPa) is Case 1c-Forced Equilibrium, close to Cases 1a and 1b (droplets); the additional evaporation cools the ambient gas, lowering the air partial pressure and the higher steam partial pressure is unable to compensate.

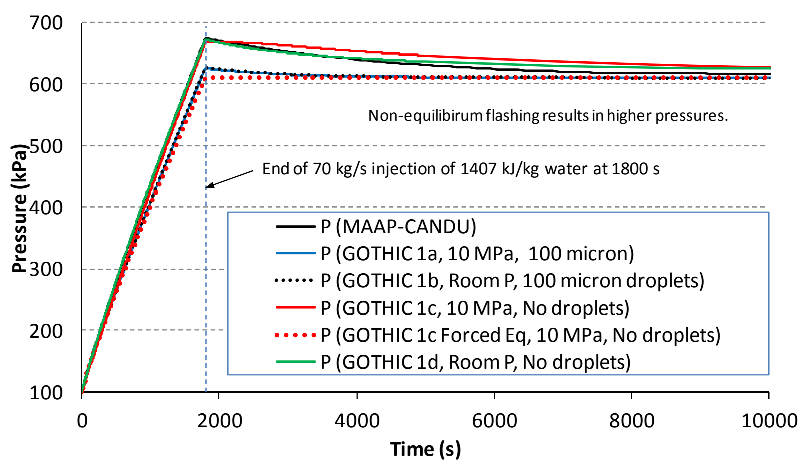

Figure 5 Benchmark 2: Node 8 total pressure - 70 kg/s flashing jet.

4.2.2 Benchmark 3: High Flow 35% Inlet Header Break Flashing Jet

Benchmark 3 is similar to Benchmark 2, but with an unsteady high-flow jet for 107 s. The flow was originally generated with the CATHENA thermalhydraulics code, for a CANDU 6 35% reactor inlet header (RIH) break. The CATHENA D_2O flows were converted to light water by maintaining the same RIH pressure, quality, liquid subcooling and vapour superheat, and by assuming the mass flows are proportional to the square root of the density. The total energy injected into containment, for the equivalent light water flow, is 99.6% of that of the heavy water flows. Figure 6 shows the resulting steam and water injection rates, and specific enthalpies. Approximately 35,000 kg of water and ~25,000 kg of steam are injected over 107 s (Figure 7).

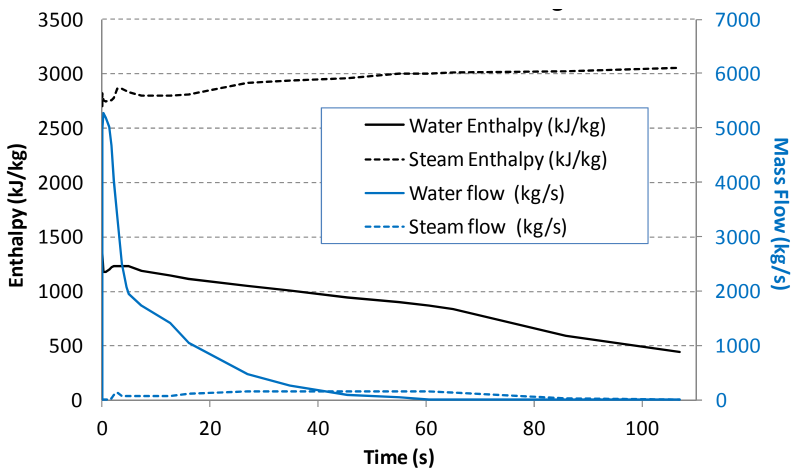

Figure 6 Benchmarks 3 and 6: Mass flows and specific enthalpies - 35% RIH break discharge.

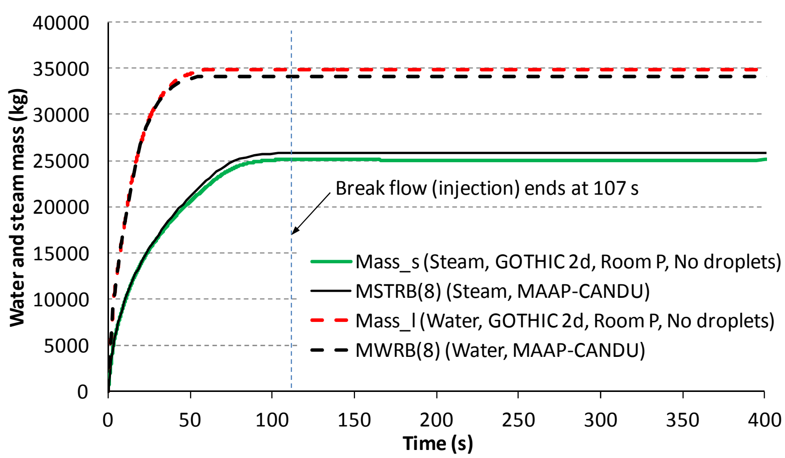

Figure 7 Benchmark 3: Node 8 steam and water masses - 35% RIH break discharge.

The ambient gas temperatures of the "near equilibrium" GOTHIC simulations are virtually identical during the injection, and are close to the liquid temperatures, particularly after the injection ceases (Figure 8). This is like Benchmark 2, since these cases model the jet with small droplets (Cases 2a and 2b) or use a forced equilibrium model (Case 2c-Forced Equilibrium). Case 2c uses the RIH pressure (10 MPa and declining) to generate the flashing conditions, after the jet water is added to the pool. Case 2d assumes the break flow flashes at the node pressure.

The ambient gas temperatures for non-equilibrium models (GOTHIC 2c and 2d, and MAAP-CANDU) exceed those of near-equilibrium models by maxima of ~65 to 90°C at the end of the break flow (107 s) and then decline (Figure 8) towards the liquid temperatures as thermal equilibrium is approached. The liquid temperatures of the GOTHIC 2d and MAAP-CANDU simulations are very close to those of the near-equilibrium models; the MAAP-CANDU liquid temperature exceeds that of Case 2d by a maximum of ~6°C at 3,000 s, before decreasing.

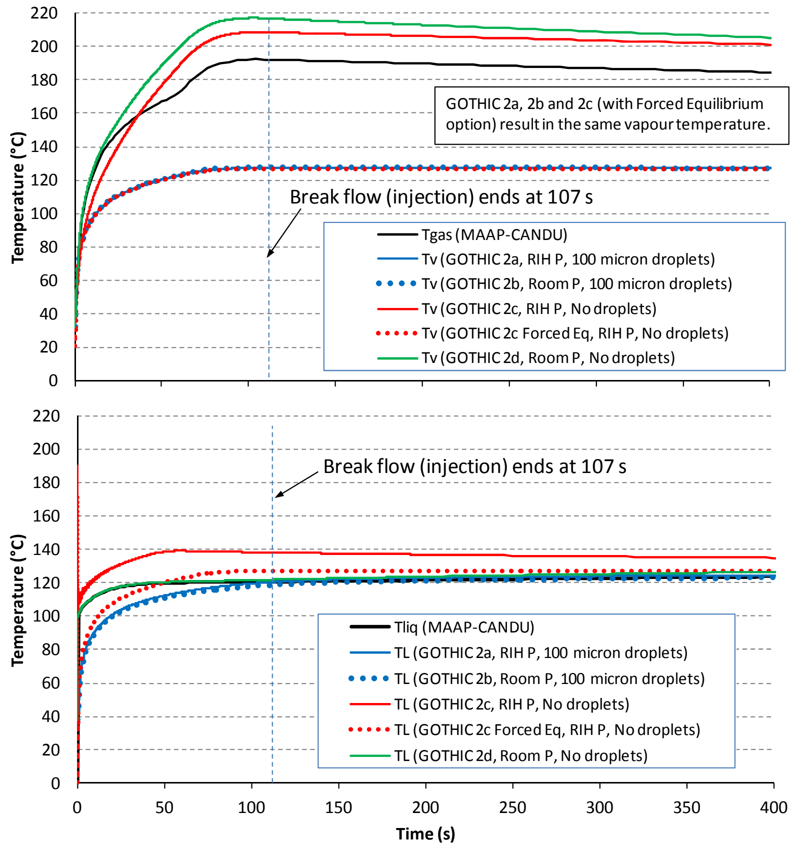

Figure 8 Benchmark 3: Node 8 gas and water temperatures - 35% RIH break discharge.

Like Benchmark 2, the relative humidity (Figure 9) rapidly increases to 100% for the near-equilibrium Cases 2a, 2b and 2c-Forced Equilibrium. The non-equilibrium GOTHIC 2c and 2d, and MAAP-CANDU simulations rapidly increase to 80-100% humidity, and then decline sharply to ~20% by the end of the break flow, because the non-equilibrium models produce less steam and also heat the atmosphere significantly more, compared to the near-equilibrium simulations. After the injection ceases, however, the ambient temperature declines, decreasing the saturation pressure, as heat transfers to the water. The water also evaporates (a slower process than flashing), increasing the partial pressure of steam and thus raising the relative humidity.

Again, the "non-equilibrium" MAAP-CANDU and GOTHIC 2c and 2d simulations generate the highest peak containment pressures (Figure 10), all occurring at the end of the break period (107 s). GOTHIC Case 2d generates the maximum peak pressure of 0.446 MPa, and MAAP-CANDU generates the lowest (0.434 MPa) of the non-equilibrium models. These pressures correspond to the ambient gas temperatures (Figure 8). GOTHIC near-equilibrium Cases 2a, 2b and 2c-Forced Equilibrium have the same response but lower peak pressures.

From Benchmarks 2 and 3, GOTHIC Cases 1d and 2d results are close to those of MAAP-CANDU, since both codes model constant-enthalpy flashing at the containment node ambient conditions. The other GOTHIC non-equilibrium model (Cases 1c and 2c, where the break pressure is set to the upstream pressure) also generates results close to those of MAAP-CANDU.

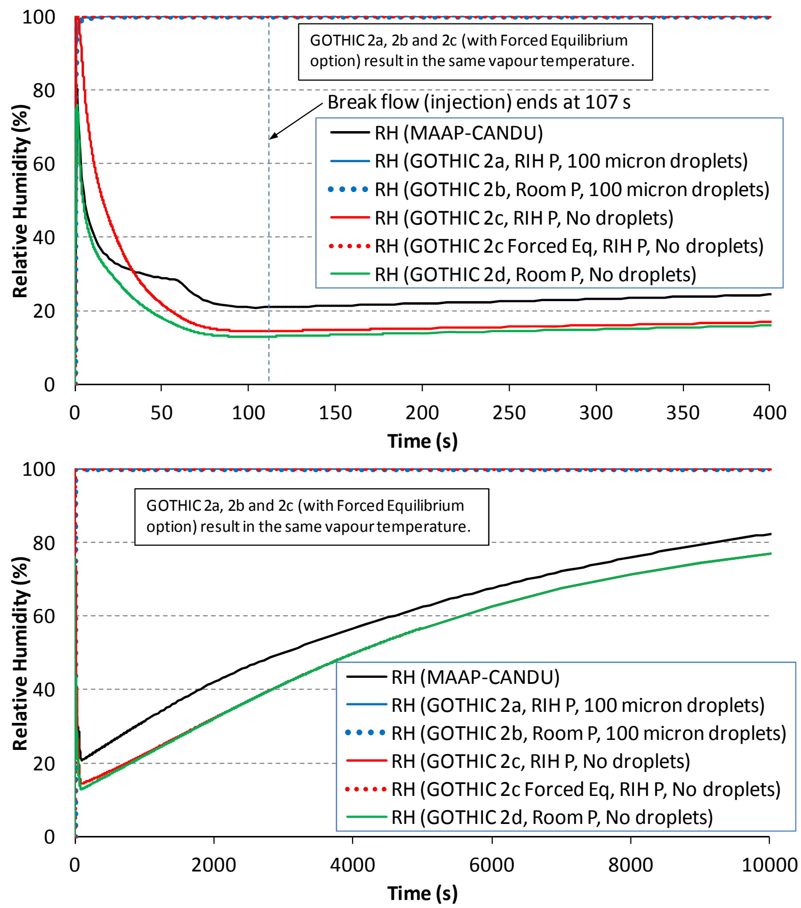

Figure 9 Benchmark 3: Node 8 relative humidity - 35% RIH break discharge.

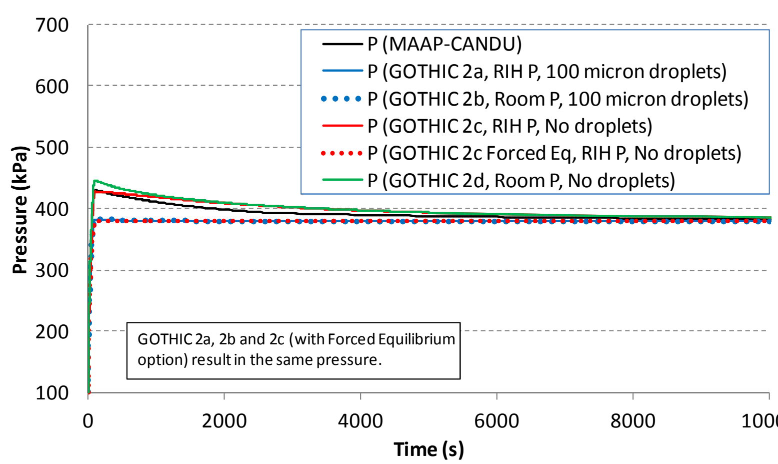

Figure 10 Benchmark 3: Node 8 total pressure - 35% RIH break discharge.

The near-equilibrium cases either use fine droplets of water or forced equilibrium, which generates similar results; the relative humidity becomes 100% almost immediately, the vapour and liquid temperatures are very close to each other, and the peak containment pressure is significantly lower. NAI recommends using the near-equilibrium flashing jet model, as in Cases 1b and 2b. However, the non-equilibrium model generates the highest containment pressures, which may be conservative from the perspective of possible containment failure.

4.3 Benchmark 4: Heat Sink Condensation and Convection

In Benchmark 4, single-sided Heat Sink 65 (concrete, vertical, 1,000 m^2 area, 0.2 m thick, 10 m high) is exposed to containment so convection and condensation heat transfer can occur. The heat transfer models are described for combined convection, radiation and condensation, as derived by Collier [8] and used in MAAP-CANDU. The process calculates the heat fluxes i) from the containment atmosphere to the condensate film, and ii) through the condensate to the heat sink surface, and iterates the interface temperature T_i, between the condensate film and the ambient atmosphere until the two heat fluxes match.

The radiation $\ddot{q}_{rad}$ and convection $\ddot{q}_{conv}$ heat fluxes are solved from the ambient gas to the heat sink surface, ignoring condensation or evaporation. For a vertical heat sink in a large volume, the natural convection Nusselt number is modeled as a function of the Rayleigh number Ra, which is the product of the Prandtl ($c_p\,\mu/k$) and Grashof (Equation 7) numbers:

$$\ddot{q}_{conv} = H_{conv}(T_\infty - T_s)\text{ , where } \mathrm{Nu} = \frac{H_{conv}\,L}{k_g} = K\,\mathrm{Ra}^n \text{ or } H_{conv} = \frac{k_g\,K\,\mathrm{Ra}^n}{L} \tag{15}$$

For Ra<10^9 coefficient K=0.555 and n=0.25; for Ra>10^9 K=0.021 and n=0.4. The gas properties are at the ambient gas conditions (T_∞, P_∞). The Grashof number uses the heat sink height L and temperature difference (T_∞ - T_s), where T_s is the heat sink surface temperature.

Radiation heat transfer between the ambient gas and heat sink is approximated by that for two infinite planes. This is simplistic, but radiation heat transfer is low, given the small temperature difference T_∞ - T_s, especially compared to the high condensation heat transfer.

$$\ddot{q}_{rad} = H_{rad}(T_\infty - T_s) = \frac{\sigma\left(T_\infty{}^4 - T_s{}^4\right)}{\left(\frac{1}{\epsilon_{gas}} + \frac{1}{\epsilon_{surf}} - 1\right)} \quad \text{or } H_{rad} = \frac{\sigma\left(T_\infty{}^2 + T_s{}^2\right)(T_\infty + T_s)}{\left(\frac{1}{\epsilon_{gas}} + \frac{1}{\epsilon_{surf}} - 1\right)} \tag{16}$$

The sensible heat transfer coefficients H_{conv} and H_{rad} are now known, and interface temperature T_i, is estimated. For a vertical wall (no water flow from other heat sinks or sprays), the average heat flux $\ddot{q}_{film}$ through a growing condensate film [8] is:

$$\ddot{q}_{film} = H_{film}(T_i - T_s) \quad \text{where} \quad H_{film} = H^*\,k_w\left(\frac{g}{\nu_w^2}\right)^{1/3} \tag{17}$$

H^* is the dimensionless heat transfer coefficient, k_w the water thermal conductivity, and ν_w the water kinematic viscosity. Water properties are calculated at the mean film temperature, $T_{film} = T_s + 0.25\,(T_i - T_s)$. H^* is based on dimensionless length L^*:

$$L^* = \frac{4\,L\,c_{p_w}\,(T_i - T_s)}{\mathrm{Pr}_w\,h'_{fg}}\left(\frac{g}{\nu_w^2}\right)^{1/3}\left(\frac{1}{1 - \rho_g/\rho_w}\right) \tag{18}$$

The specific heat of water c_{p_w}, Prandtl number Pr_w, and densities of saturated steam ρ_g and water ρ_w are also solved at T_{film}. The enthalpy of steam condensation h_{fg} is modified to account for cooling in the water film, $h'_{fg} = h_{fg} + 0.68\,c_{p_w}\,(T_i - T_s)$. For L^*<14,350, laminar film condensation is assumed. For simplicity H^* is also assumed independent of the Prandtl number (except within L^*), and was correlated as:

$$H^* = 10^Y \quad \text{where} \quad Y = 0.129466 - 0.25566 \log_{10}(L^*) \tag{19}$$

Additional correlations of Y are used in MAAP-CANDU for turbulent film condensation. However, for the height (L=10 m) of Heat Sink 65, and the typical containment conditions of the current benchmarking exercises, laminar film condensation is dominant.

With a known heat sink surface temperature T_s and ambient gas conditions (T_∞, P_∞, $P_{stm\infty}$), the interface temperature T_i is estimated and used to solve the dimensionless heat transfer coefficient H^* and then the average heat flux $\ddot{q}_{film}$ through the condensate film. The total heat flux $\ddot{q}_{atm}$ from the atmosphere to the condensate is a combination of sensible and latent heat transfer [8]:

$$\begin{aligned} \ddot{q}_{atm} &= \ddot{q}_{rad} + \ddot{q}_{conv} + \ddot{q}_{cond} \\ &= (H_{rad} + H_{conv})(T_\infty - T_i) + H_m\, M_{stm}\left(h_{stm,\infty} - h_w\right)(P_{stm,\infty} - P_{stm,i}) \end{aligned} \tag{20}$$

Sensible heat transfer coefficients H_{conv} and H_{rad} were derived in Equations 15 and 16, M_{stm} is the steam molecular weight , $h_{stm,\infty}$ the ambient steam enthalpy , and h_W the condensate enthalpy at T_{film}. $P_{stm,\infty}$ is the ambient steam partial pressure, and $P_{stm,i}$ is the saturation pressure at the estimated interface temperature T_i. The difference in partial pressures drives the condensation, much like the difference in temperature drives sensible heat transfer. Mass transfer coefficient H_m is evaluated using Reynolds' analogy between convective heat transfer and mass transfer [8]:

$$H_m = \frac{H_{conv}}{c_{p,\infty}\, P_{am}\, M_{stm}} \left(\frac{\mathrm{Pr}}{\mathrm{Sc}}\right)^{2/3} \tag{21}$$

where the Prandtl and Schmidt numbers are evaluated at the ambient gas conditions, as is the specific heat $c_{p,\infty}$. The ambient pressure P_{am} is the log mean difference of the partial pressures of the non-condensable gas (air) at the interface and the bulk conditions:

$$P_{am} = \frac{P_{air,i} - P_{air,\infty}}{\ln\left(\frac{P_{air,i}}{P_{air,\infty}}\right)} = \frac{P_{stm,\infty} - P_{stm,i}}{\ln\left(\frac{P - P_{stm,i}}{P - P_{stm,\infty}}\right)} \tag{22}$$

Now knowing the mass transfer coefficient H_m, Equation 20 is solved for the total heat flux $\ddot{q}_{atm}$ from the atmosphere to the condensate. Equation 17 is solved for the total heat flux $\ddot{q}_{film}$ through the condensate film. An iterative solution is used to adjust T_i until $\ddot{q}_{atm} = \ddot{q}_{film}$.

4.3.1 Benchmark 4: Condensation and Convection of Quiescent Volume

In Benchmark 4, vertical single-sided Heat Sink 65 is initially at 25°C. The initial conditions are 300 kPa (abs), 133.5°C, and 60% relative humidity, with no initial water pool and no steam discharge into Node 8. The MAAP-CANDU and GOTHIC simulations run to 50,000 s.

The two simulations are similar (Figure 11). The total pressure declines smoothly from 300 to 182 kPa, and the gas temperature from 133.5 to 92.5°C. By 1,625 s, the relative humidity increases to 100%. Condensation rates (Figure 12) are virtually identical between simulations; some occasional spikes occur during the MAAP-CANDU run, but these have no consequence upon the integrated results (relative humidity, temperature, pressure). The differences between the MAAP-CANDU and GOTHIC simulations are minor and inconsequential.

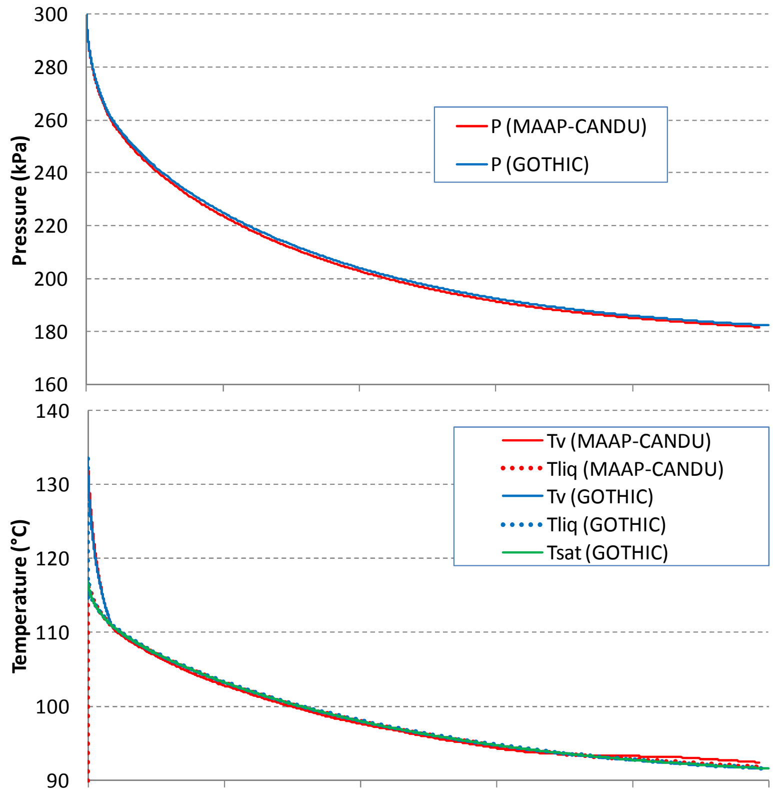

Figure 11 Benchmark 4: Node 8 pressure and gas temperature - Heat sink active.

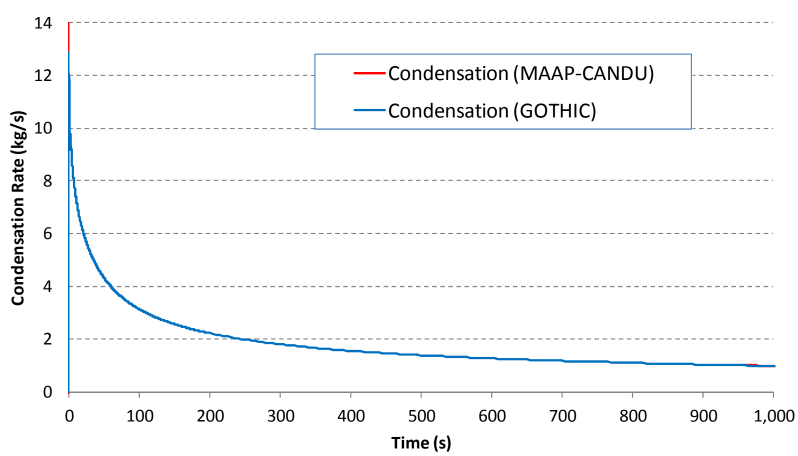

Figure 12 Benchmark 4: Node 8 condensation rates - Heat sink active, no injection.

4.4 Benchmarks 5 and 6: Flashing Jet Injection with Heat Sink

The final benchmarks are repeats of Benchmark 2 (steady injection of saturated water and steam) and Benchmark 3 (35% RIH break), except with Heat Sink 65 active. Again, Node 8 is adiabatic, except for Heat Sink 65. Thus any water pool can only cool by evaporation to the Node 8 atmosphere. Two GOTHIC break discharge models are used in these simulations:

a) The recommended GOTHIC break ("GBreak") discharge method: flashing the jet at the downstream conditions, adding the resulting steam to Node 8 and adding the unflashed liquid as 100 micron droplets, like in GOTHIC Cases 1b and 2b.

b) The MAAP-CANDU break ("MBreak") discharge method: flashing the jet at the downstream conditions, adding the resulting steam to the vapour phase in containment and the unflashed liquid directly to the water pool, as used in GOTHIC Cases 1d and 2d.

4.4.1 <u>Benchmark 5: Steady-State Flashing Jet with Heat Sink</u>

In Benchmark 5, 70 kg/s of saturated water/steam was injected for 1,800 s, with similar results to Benchmark 2 (without a heat sink, Section 4.2.1). Pressures (Figure 13) are about 20 kPa lower than without the heat sink (Figure 5), because of condensation on Heat Sink 65.

Likewise, Benchmark 5 temperatures (Figure 14) are lower than without a heat sink (Figure 3). The GOTHIC-MBreak vapour and liquid temperatures are all above the saturation temperature (based on the steam partial pressure), indicating the interface area (floor surface) is insufficient to permit enough evaporation to reach equilibrium. The MAAP-CANDU vapour temperature is also above the saturation temperature, but the MAAP-CANDU liquid temperature is below saturation. This indicates that MAAP-CANDU calculated more evaporation than GOTHIC-MBreak, which is reflected in the slightly higher MAAP-CANDU pressure and steam mass.

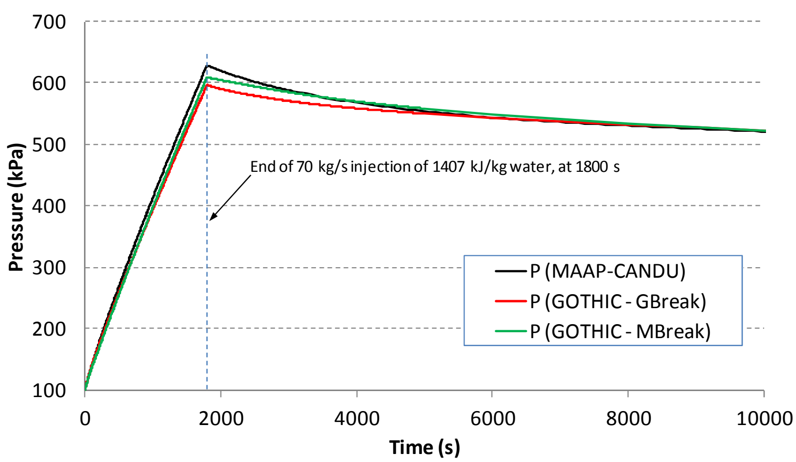

Figure 13 Benchmark 5: Node 8 total pressure - 70 kg/s flashing jet + heat sink.

The GOTHIC and MAAP-CANDU condensation rates (Figure 15) are similar after ~4,500 s. During the break discharge (0 to 1,800 s), both GOTHIC-MBreak and MAAP-CANDU show a strong net evaporation (flashing within Node 8), whereas the GOTHIC-GBreak model shows most evaporation occurs outside Node 8 (flashing prior to being added to Node 8). The GOTHIC-MBreak model shows strong oscillations in the evaporation, perhaps from numerical instabilities, but oscillates about the MAAP-CANDU evaporation rate. The total steam mass (Figure 16) shows GOTHIC-MBreak predicted less evaporation than MAAP-CANDU.

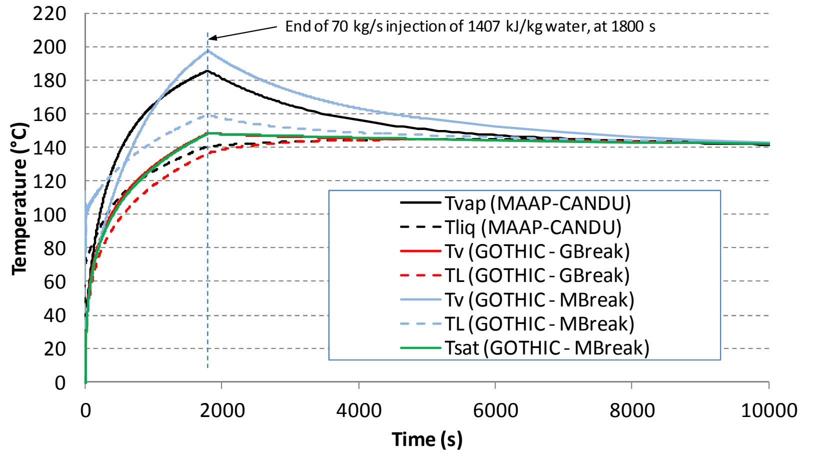

Figure 14 Benchmark 5: Node 8 gas and water temperatures - 70 kg/s flashing jet + heat sink.

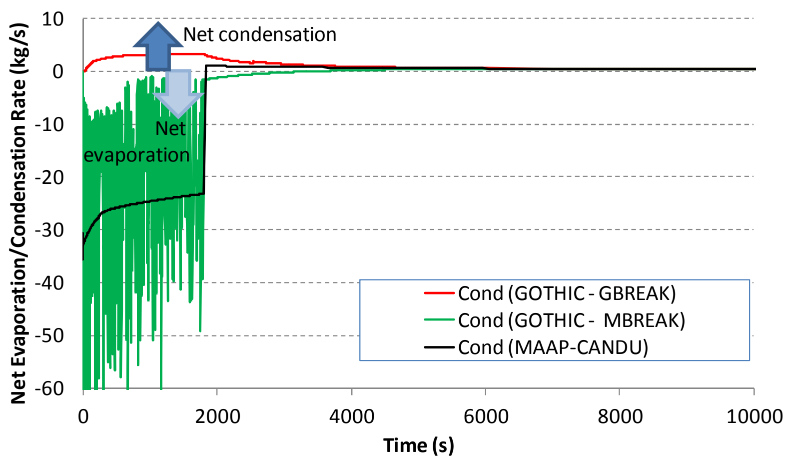

Figure 15 Benchmark 5: Node 8 net evaporation/condensation - 70 kg/s flashing jet + heat sink.

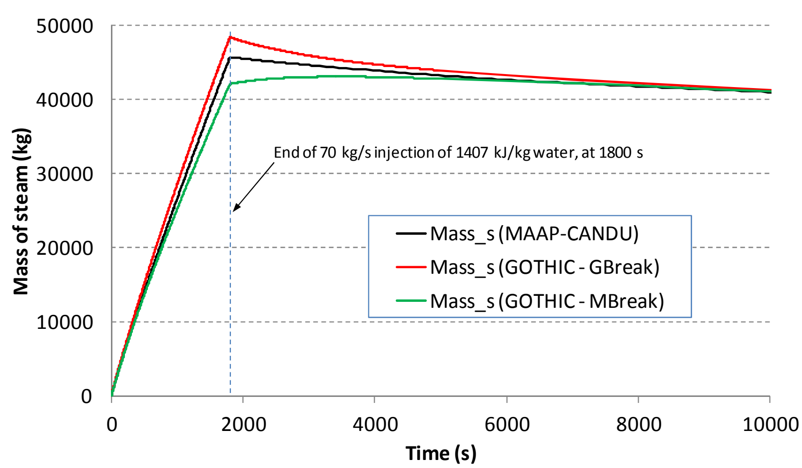

Figure 16 Benchmark 5: Node 8 steam mass - 70 kg/s flashing jet + heat sink.

The main differences between GOTHIC-GBreak and MAAP-CANDU / GOTHIC-MBreak are:

- GOTHIC-GBreak: unflashed break liquid is added as 100 micron droplets, giving a large interfacial area and thus permitting the vapour and droplets to reach thermal equilibrium.
- The vapour temperature for GOTHIC-GBreak remains at the saturation temperature (based on the partial pressure of the steam).
- The GOTHIC-GBreak liquid is sub-cooled because any new liquid is from condensate and gravitational settling of cooled droplets from the jet, which have partially evaporated and are thus cooled before they settle into the liquid pool.
- GOTHIC-GBreak has the highest mass of steam, and the lowest peak pressure, because the vapour remains at the saturation temperature (no superheating).

4.4.2 Benchmark 6: High Flow 35% Inlet Header Break Flashing Jet with Heat Sink

The final benchmark adds the 35% RIH break discharge into Node 8 (i.e., 0 – 107 s), and includes Heat Sink 65. The general result trends are similar to those of Benchmark 3 (i.e., RIH break discharge without a heat sink, Section 4.2.2).

The peak pressures (Figure 18) occur at the end of the break discharge period, and again the MAAP-CANDU and GOTHIC-MBreak simulations have the highest values. However, the peak values are about 20 kPa lower than when no heat sink is modelled (Figure 10). The presence of the heat sink further condenses steam, and thus the final pressure (at 10,000 s) is approximately 70 kPa lower in Benchmark 6 compared to Benchmark 3.

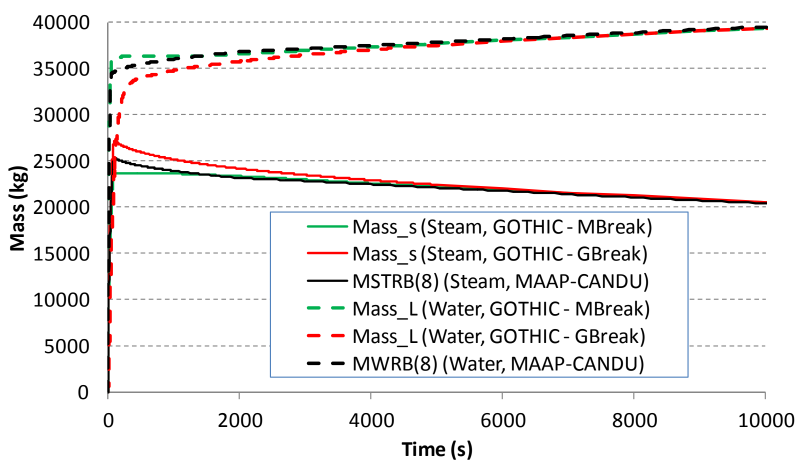

Figure 17 Benchmark 6: Node 8 steam and water masses - 35% RIH break + heat sink.

The peak liquid and gas (vapour) temperatures (Figure 19) are lower than those in Benchmark 3 (Figure 8), due to presence of the heat sink. Evidently the heat sink is promptly used by the node atmosphere, reflecting the lumped containment node modeling, but is non-conservative in that it would lead to lower containment pressures. For a large discharge of steam, such as the 35% RIH break in Benchmarks 3 and 6, the rapid response of condensing surfaces is more appropriate.

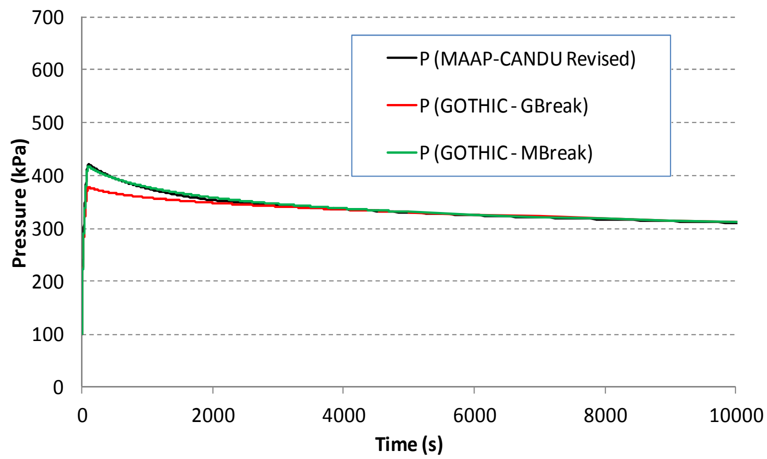

Figure 18 Benchmark 6: Node 8 total pressure - 35% RIH break + heat sink.

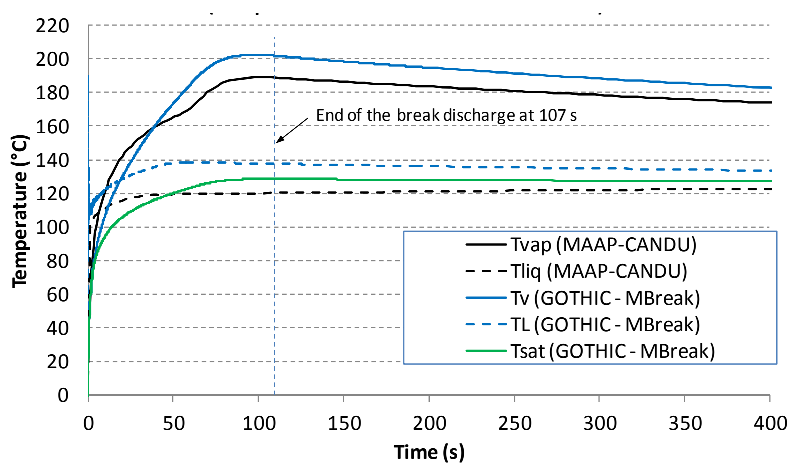

Figure 19 Benchmark 6: Node 8 gas and water temperatures - 35% RIH break + heat sink.

5. Summary

Six simple single-node lumped-parameter containment benchmarks were performed for this paper, comparing results from MAAP-CANDU 4.0.7B with those available in GOTHIC 7.2. The benchmarks all use a large (19,809 m^3) rectangular adiabatic volume. Analytical solutions (for superheated steam injection) and the applicable theory behind models of flashing jets, pool evaporation and condensation are also discussed. The specific benchmarks are:

1. Continuous injection of superheated steam into a dry room (includes analytical solution).
2. Steady injection of flashing jet for 1,800 s into a dry room.
3. Injection of flashing jet (35% RIH break in a CANDU 6) into a dry room.
4. Quiescent convection and condensation heat transfer to a single large vertical heat sink, beginning at hot and humid initial conditions.
5. Like Benchmark 2, plus condensation / convection to heat sink from Benchmark 4.
6. Like Benchmark 3, plus condensation / convection to heat sink from Benchmark 4.

The containment pressure (peak or at a specific time) is used to compare the MAAP-CANDU, GOTHIC and (in Benchmark 1) analytical solutions (Table 2). The pressure difference (MAAP-CANDU – GOTHIC) is listed as a fraction of the GOTHIC-generated pressure.

Table 2: Pressure Figure-of-Merit

Benchmark	**Code**	**Pressure P_{GOTHIC} (Pa)**	$\frac{P_{MAAP-CANDU} - P_{GOTHIC}}{P_{GOTHIC}}$
1 Superheated steam jet		At 500 s:	
	MAAP-CANDU	294,321	0%
	GOTHIC	293,912	+0.1%
	Analytical Solution	295,492	-0.4%
		At 10,000 s:	
	MAAP-CANDU	3,744,590	0%
	GOTHIC	3,746,321	+0.05%
2 Flashing jet (1800 s)		Peak at ~1800 s:	
	MAAP-CANDU	674,070	0%
	GOTHIC 1a	625,534	+7.8%
	GOTHIC 1b	626,906	+7.5%
	GOTHIC 1c	668,327	+0.9%
	GOTHIC 1c-Forced Equilibrium	609,924	+10.5%
	GOTHIC 1d	672,865	+0.2%
3 Flashing jet (RIH break)		Peak at ~107 s:	
	MAAP-CANDU	430,018	0%
	GOTHIC 2a	381,840	+12.6%
	GOTHIC 2b	383,481	+12.1%
	GOTHIC 2c	427,574	+0.6%
	GOTHIC 2c-Forced Equilibrium	379,191	+13.4%
	GOTHIC 2d	446,083	-3.6%
4 Quiescent volume with heat sink		At 1,000 s:	
	MAAP-CANDU	269,270	0%
	GOTHIC	270,071	-0.3%
		At 50,000 s:	
	MAAP-CANDU	181,458	0%
	GOTHIC	182,458	-0.5%
5 Flashing jet (1800 s) with heat sink		Peak at ~1800 s:	
	MAAP-CANDU	627,588	0%
	GOTHIC (MAAP-CANDU break)	608,845	+3.1%
	GOTHIC (GOTHIC break)	596,267	+5.3%
6 Flashing jet (RIH break) with heat sink		Peak at ~107 s:	
	MAAP-CANDU	421,137	0%
	GOTHIC (MAAP-CANDU break)	417,114	+1.0%
	GOTHIC (GOTHIC break)	377,900	+11.4%

The behaviours of the superheated vapour, condensation and convection models are very close; the absolute values of the pressure differences are less than 0.5% of the pressure. The main differences between codes occur with the flashing models. MAAP-CANDU models a flashing jet assuming a constant break enthalpy, dividing the flow between saturated water and steam based upon the saturation enthalpies at the downstream (node) pressure. When GOTHIC uses a similar non-equilibrium fashion flashing model, then similar results are obtained; some small differences can be expected (e.g., slightly lower pressure, higher vapour and liquid temperatures, lower flashing rate and lower steam mass) in the short term before attaining thermal equilibrium.

However, when MAAP-CANDU is compared against the recommended GOTHIC flashing jet model, more significant differences can be expected:

- The scenarios considered in this study show that MAAP-CANDU predicts a higher peak pressure (up to ~13%) than GOTHIC.
- GOTHIC vapour temperatures remain at the saturation temperature, whereas MAAP-CANDU predicts a high degree of superheat (up to 60°C superheat for a 35% RIH break).
- GOTHIC predicts about 5% higher steam concentration than MAAP-CANDU.

The recommended GOTHIC flashing jet model uses a near-equilibrium approach, where any liquid remaining post-flashing is assumed to be sprayed out as 100 micron droplets, which promptly evaporate due to the very large surface area of the droplets. However, the non-equilibrium model generates the highest containment pressures, which may be conservative from the perspective of possible containment failure.

MAAP-CANDU simulates an entire CANDU station during a postulated severe accident, including the core, heat transport system, moderator, reactor vault, fission product behaviour, safety systems and containment. MAAP-CANDU does not have the model capabilities or detail that are available in the GOTHIC containment analysis code, but the MAAP-CANDU lumped-parameter containment models show good agreement with the equivalent GOTHIC models.

6. References

[1] P.M. Mathew, S.M. Petoukhov and M.J. Brown, *An Overview of MAAP4-CANDU Code*, 28th Annual Conference of the Canadian Nuclear Society, 2007 June 3-6.

[2] S.M. Petoukhov, N. Karancevic, A.C. Morreale, C.Y. Paik, M.J. Brown and C. Cole, *Development of the Graphical Animation Interactive Feature to Assess MAAP-CANDU Simulation Results*, 7th International Conference on Modelling and Simulation in Nuclear Science and Engineering (7ICMSNSE), 2015 October 18-21.

[3] T.L. George et al., *Containment Analysis with GOTHIC*, ASME 27th National Heat Transfer Conference, 1991 July.

[4] M.J. Brown, S.M. Petoukhov and P.M. Mathew, *Influence of Coolant Phase Separation on Event Timing During a Severe Core Damage Accident in a Generic CANDU 6 Plant*, Workshop on Evaluation of Uncertainties In Relation To Severe Accidents and Level 2 Probabilistic Safety Analysis, 2005 November 7-9.

[5] S.M. Petoukhov and T.H. Nguyen, *Comparison of Containment Dousing System Response for a CANDU 6 Station Blackout Sequence Using MAAP4-CANDU (v4.0.7) and GOTHIC (v7.2b)*, 2015 International Congress on Advances in Nuclear Power Plants (ICAPP), 2015 May 3-6.

[6] S.M. Petoukhov, B. Awadh, T.H. Nguyen and P.M. Mathew, *Comparison of Containment Response for a CANDU 6 Station Blackout Sequence Using MAAP4-CANDU (v4.0.7) and GOTHIC (v7.2b)*, 20th International Conference on Nuclear Engineering and ASME 2012 Power Conference ICONE20 POWER2012, 2012 July 30 – August 3.

[7] K.B. Katsaros, W.T. Jiu, J.A. Businger and J.E. Tillman, *Heat Transport and Thermal Structure in the Interfacial Boundary Layer Measured in an Open Tank of Water in Turbulent Free Convection*, Journal of Fluid Mechanics, Vol. 83 pp. 311-338, 1977.

[8] J.G. Collier, *Convective Boiling and Condensation*, McGraw-Hill, pp. 311-319, 1972.

7. Acronyms

AECL	Atomic Energy of Canada Limited
CANDU	CANada Deuterium Uranium reactor
CNL	Canadian Nuclear Laboratories, formerly AECL
CNSC	Canadian Nuclear Safety Commission
COG	CANDU Owners Group
ECC	Emergency Core Cooling system
FAI	Fauske and Associates, Inc. (Burr Ridge, IL, USA)
FP	Fission Product
GOTHIC	Generation of Thermal Hydraulic Information in Containments
GRAPE	GRaphical Animation Package Extension
IST	Industry Standard Toolset
LWR	Light Water Reactor
MAAP	Modular Accident Analysis Program (generic term for the suite of codes)
MAAP-CANDU	Modular Accident Analysis Program, CANDU version
PHTS	Primary Heat Transport System
SAM	Severe Accident Management